Journal of Magnetic Resonance **142,** 313–322 (2000)
doi:10.1006/jmre.1999.1946, available online at http://www.idealibrary.com on IDEAL®

A *k*-Space Analysis of MR Tagging

William S. Kerwin and Jerry L. Prince

Department of Electrical and Computer Engineering, The Johns Hopkins University, Baltimore, Maryland 21218

Received June 23, 1999; revised September 23, 1999

We present a *k*-space approximation that directly relates a pulse sequence to its residual pattern of *z*-directed magnetization M_z, in a manner akin to the *k*-space approximation for small tip-angle excitation. Our approximation is particularly useful for the analysis and design of tagging sequences, in which M_z is the important quantity—as opposed to the transverse magnetization components M_x and M_y considered in selective excitation. We demonstrate that our approximation provides new insights into tagging, can be used to design novel tag patterns, and, more generally, may be applied to selective presaturation sequences for purposes other than tagging.

Key Words: **tagging; pulse sequences; small tip-angle approximation; *k* space; presaturation.**

1. INTRODUCTION

Magnetic resonance tagging is a valuable, noninvasive tool for analyzing tissue motion *in vivo* (*1–3*). The act of tagging produces a variable brightness pattern in subsequent images and the deformation of that pattern over time clearly indicates tissue motion. Because tag patterns are induced using pulse sequences similar to those used for selective excitation, selective excitation theory may be used to relate pulse sequences to tag patterns. In particular, the *k*-space approximation for small tip-angle excitation (*4*) has been used to provide a simple explanation of tagging (*3*), as well as to design actual pulse sequences for novel tag patterns (*5*).

The excitation *k*-space approximation is effective in this capacity because it provides, through Fourier theory, an inherently satisfying and comprehensible relationship between pulse sequences and excitation patterns. For tagging sequences, however, use of the excitation *k*-space approach leads to several problematic issues. Most notably, the *k*-space approximation only addresses the M_x and M_y components of magnetization, whereas tag patterns encode the M_z component. Thus, pulse sequence design for tagging requires (1) the identification of a pattern in M_x and M_y that corresponds to the desired tag pattern in M_z, and (2) the design of a pulse sequence to create that corresponding pattern. Such a two-step process is clouded by the nonlinear relationship among M_x, M_y, and M_z as well as issues that arise in pulse sequence design for M_x and M_y that do not affect M_z. For example, the phase of the resulting excitation plays no role in determining M_z.

To avoid the shortcomings of the *k*-space approximation with respect to tagging, we derive here an extension of the theory that directly relates a pulse sequence to the resulting pattern in M_z. This extension provides an approximate expression for the *k*-space encoding of M_z analogous to the existing small tip-angle approximation for M_x and M_y. We demonstrate that our result predicts tag patterns more accurately than the excitation *k*-space approach, while maintaining a simple Fourier transform relationship between pulse sequence and pattern. We also show that the approximation can be used to simplify pulse sequences for complicated tag patterns such as variable separation tags (see (*5*)), that it works equally well in multiple dimensions, and that it is readily applicable to the related area of selective presaturation.

2. BACKGROUND

2.1. Tagging

At a fundamental level, tags are created by an RF/gradient pulse sequence followed by a strong gradient saturation pulse. Any magnetization components tipped into the *xy* plane by the pulse sequence are effectively removed by the dephasing effects of the saturation pulse. The residual M_z component of magnetization is the tag pattern. In subsequent images, the underlying proton density appears multiplied or modulated by this tag pattern. The resulting pattern is transient, fading over time as M_z recovers with longitudinal relaxation. Before fading, the tag pattern moves with tissue motion, providing features that may be tracked over a sequence of images. This motion tracking characteristic of tags has made them quite useful for studying cardiac function (*3, 6*).

Tagging is best illustrated by an example of a popular technique known as spatial modulation of magnetization (SPAMM) (*2*). SPAMM is a tagging sequence consisting of alternating nonselective RF pulses and identical gradient pulses. For example, Fig. 1a shows a 1-1 SPAMM sequence in which two RF pulses with associated tip-angles of 45° are separated by a gradient pulse oriented in the x direction with total area G. After the first RF pulse, the gradient pulse induces a phase dispersion across the sample of Φx, where $\Phi = \gamma G$ and γ is the gyromagnetic ratio. Then, at positions where Φx is an even multiple of π, the second RF pulse adds constructively

1090-7807/00 $35.00

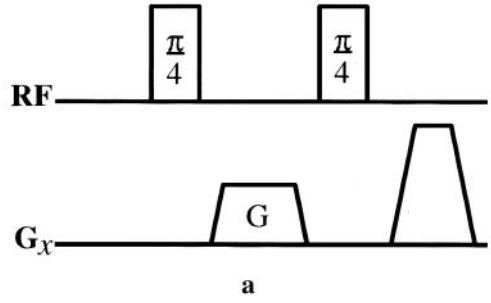

a

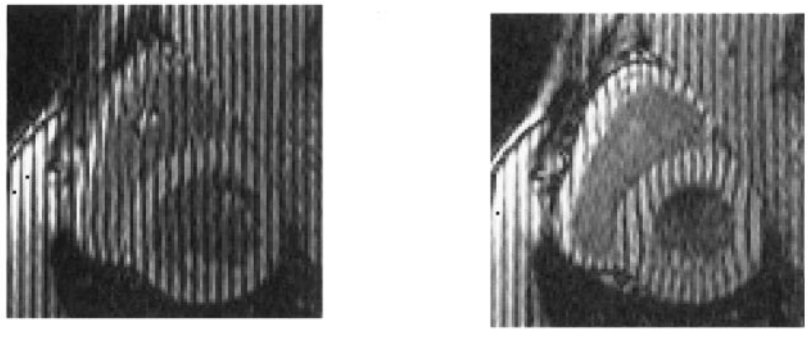

b c

FIG. 1. Demonstration of SPAMM tags with (a) the pulse sequence for generating 1-1 SPAMM tags, (b) an image of a human heart with undeformed tags, and (c) an image with tags deformed by partial LV contraction.

with the first for a total tip of 90°, leaving no residual M_z. Thus, the resulting pattern consists of regularly spaced dark bars located where $x = 2m\pi/\Phi$. The complete transverse tag brightness profile is

$$M_z(x) = \tfrac{1}{2} - \tfrac{1}{2}\cos(\Phi x). \quad [1]$$

An image modulated by this pattern is shown in Fig. 1 along with a second image showing the effect of motion on the pattern. For SPAMM sequences with more than two RF pulses, the dark parallel bars are more sharply defined (*7*).

Other pulse sequences producing similar patterns have been proposed using delays alternating with nutations for tailored excitation (DANTE) (*8*). Somewhat more complicated sequences have been proposed for patterns of dark bars limited to localized regions (*9*) and with variable separations between bars (*5*). Finally, very specific patterns can be generating by adapting approaches for regional volume excitation such as the completely arbitrary regional volume excitation (CARVE) algorithm (*10*).

2.2. Bloch Equation Solutions

To design pulse sequences for tagging, a method is needed to solve and/or invert the Bloch equation for M_z. Neglecting relaxation, the Bloch equation in the rotating frame is

$$\begin{bmatrix} \dot{M}_x \\ \dot{M}_y \\ \dot{M}_z \end{bmatrix} = \gamma \begin{bmatrix} 0 & \mathbf{G}\cdot\mathbf{x} & -B_{1,y} \\ -\mathbf{G}\cdot\mathbf{x} & 0 & B_{1,x} \\ B_{1,y} & -B_{1,x} & 0 \end{bmatrix} \begin{bmatrix} M_x \\ M_y \\ M_z \end{bmatrix}, \quad [2]$$

where $\mathbf{G}$ is the applied gradient field, $\mathbf{x}$ is the spatial position, and $B_1 = B_{1,x} + iB_{1,y}$ is the applied RF field. In this equation, M_x, M_y, and M_z as well as $\mathbf{G}$ and B_1 are all implicit functions of time.

Although the Bloch equation does not in general have an analytic solution, it can be solved numerically to an arbitrary degree of accuracy (e.g., (*11, 12*)). The numerical solution can also be inverted to obtain the fields $\mathbf{G}$ and B_1 that produce a desired pattern of M_z. In the special case of SPAMM sequences, an analytic solution exists and has the form

$$M_z(x) = \sum_{m=0}^{N-1} \alpha_m \cos(m\Phi x), \quad [3]$$

where N is the number of RF pulses used, Φ is determined by the size of the gradient pulses, and $\alpha_0, \ldots, \alpha_{N-1}$ are coefficients determined by the sizes of the RF pulses (*11, 13*).

The drawback of such exact or nearly exact solutions is that they involve complicated expressions that often do not provide

useful insights into the relationship between the pulse sequence and the resulting pattern. For the SPAMM sequence in particular, this complexity shows up in the expressions for the coefficients $\alpha_0, \ldots, \alpha_{N-1}$. For example, the rather daunting analytic expression for a SPAMM pattern generated with only three RF pulses is

$$\begin{aligned} M_z(x) = &[\cos\theta_1\cos\theta_2\cos\theta_3 + \tfrac{1}{2}(1 - \cos\theta_2)\sin\theta_1\sin\theta_3] \\ &- [\sin\theta_2\sin(\theta_1 + \theta_3)]\cos(\Phi x) \\ &- [\tfrac{1}{2}(1 + \cos\theta_2)\sin\theta_1\sin\theta_3]\cos(2\Phi x), \end{aligned} \quad [4]$$

where θ_1, θ_2, and θ_3 are the tip angles associated with the three RF pulses (*13*). Such complicated relationships make it difficult to specify and utilize optimality criteria. For example, an important consideration in tagging is to apply the pattern rapidly because the underlying object is moving. Exact solutions for a given pattern can be found, but it may be difficult to tell whether there is an alternative pulse sequence that produces nearly the same pattern in significantly less time.

Because tagging rarely involves tipping magnetization vectors by more than 90°, tagging sequences may be analyzed with the small tip-angle approximation (*14*), which bypasses many of the complexities of the exact solutions. The small tip-angle approximation is derived by assuming a constant M_z, which we normalize to 1. Then, the Bloch equation may be written only in terms of the transverse magnetization $M_{xy} = M_x + iM_y$ as

$$\dot{M}_{xy}(\mathbf{x}, t) \approx -i\gamma\mathbf{x}\cdot\mathbf{G}(t)M_{xy}(\mathbf{x}, t) + i\gamma B_1(t). \quad [5]$$

Solving this differential equation for any position $\mathbf{x}$ and time t yields

$$M_{xy}(\mathbf{x}, t) \approx i\gamma\int_0^t B_1(s)e^{i\mathbf{x}\cdot\mathbf{k}(s,t)}ds, \quad [6]$$

where

$$\mathbf{k}(s, t) = -\gamma\int_s^t \mathbf{G}(u)du. \quad [7]$$

We explicitly include time as a variable in Eq. [6] because the expression is generally accurate at any time t in the pulse sequence. For a pulse sequence applied between 0 and T, the final transverse magnetization, which we denote as simply $M_{xy}(\mathbf{x})$, is found by evaluating Eq. [6] for $t = T$.

The final transverse magnetization computed by the small tip-angle approximation has also been formulated using a *k*-space approach (*4*). In this approach, a "path" through *k*-space is defined by

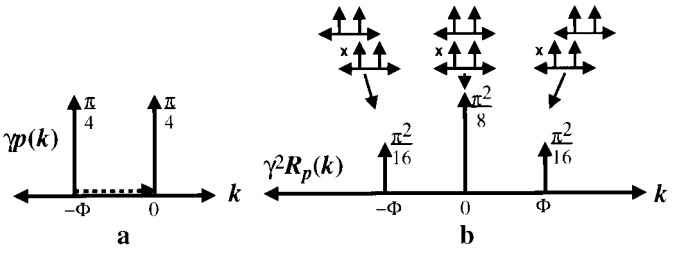

FIG. 2. The 1-1 SPAMM sequence with a total tip angle of $\pi/2$ has (a) a *k*-space path $p(k)$ consisting of two impulses, and (b) a *k*-space autocorrelation function $R_p(k)$, which is computed by shifting and multiplying the *k*-space path to obtain three impulses.

$$p(\mathbf{k}) = \int_0^T B_1(s)\delta(\mathbf{k}(s, T) - \mathbf{k})ds, \quad [8]$$

where the dimensionality of $\mathbf{k}$ is nominally 3, but may be less than 3 for some pulse sequences. With this definition, the final ($t = T$) transverse magnetization may be evaluated as

$$M_{xy}(\mathbf{x}) \approx i\gamma\int_{\mathbf{K}} p(\mathbf{k})e^{i\mathbf{x}\cdot\mathbf{k}}d\mathbf{k}, \quad [9]$$

that is, the resulting transverse magnetization and the *k*-space path are related by the Fourier transform, a concept commonly referred to as encoding *excitation k-space.*

3. METHOD: AN APPROXIMATION FOR M_z

For most tagging sequences, Eq. [9] provides a reasonable approximation of the resulting transverse magnetization M_{xy} prior to the saturation pulse. It does not, however, provide a direct, accurate expression for the tag pattern itself. The failure of excitation *k*-space to explain tagging is clearly demonstrated by a *k*-space analysis of the SPAMM sequence described in Section 2. For a SPAMM sequence with N RF pulses, the 1D path through *k*-space is given by

$$p(k) = \frac{1}{\gamma}\sum_{m=1}^{N}\theta_m\delta(k - (N - m)\Phi), \quad [10]$$

where θ_m is the tip angle (in radians) of the mth RF pulse and, again, $\Phi = \gamma G$. See Fig. 2a for an example of a SPAMM path. Examining Eq. [10], we see that SPAMM paths are, in general, sequences of N equally spaced impulse functions.

At first glance, this analysis suggests that transforming the SPAMM pattern into *k*-space by taking its Fourier transform should result in a sequence of N impulse functions. The true *k*-space representation of the SPAMM tag pattern—found by taking the Fourier transform of Eq. [3]—is, on the other hand,

a symmetric series of $2N - 1$ impulses. This number of impulses arises because each of the $N - 1$ cosine terms in Eq. [3] accounts for two frequency domain impulses, and the DC term ($m = 0$) accounts for one. This analysis begs the question that if the true k-space representation has $2N - 1$ symmetric impulses, why does the k-space path have only N impulses that are not necessarily symmetric? The primary reason is, of course, that the excitation k-space approach was not derived to predict M_z. In fact, the derivation depends on the assumption that $M_z(\mathbf{x}) = 1$ for all **x.** The excitation k-space approximation is therefore unsuitable for accurately predicting tag patterns.

To provide an accurate approximation for M_z that *is* suitable for predicting tag patterns, we note that an analytic expression for $M_z(\mathbf{x}, t)$ is possible if $M_{xy}(\mathbf{x}, t)$ is known for all time. The expression is determined by the bottom line of the Bloch equation, which may be written

$$\dot{M}_z(\mathbf{x}, t) = \tfrac{1}{2} i\gamma(\bar{B}_1(t) M_{xy}(\mathbf{x}, t) - B_1(t)\bar{M}_{xy}(\mathbf{x}, t)), \quad [11]$$

where the bar denotes a complex conjugate. To approximate $M_z(\mathbf{x}, t)$, we replace $M_{xy}(\mathbf{x}, t)$ by the small tip-angle approximation (Eq. [6]) and integrate Eq. [11] from 0 to t. The solution is

$$M_z(\mathbf{x}, t) \approx 1 - \tfrac{1}{2}\left| \gamma \int_0^t B_1(s) e^{i\mathbf{x}\cdot\mathbf{k}(s,t)} ds \right|^2, \quad [12]$$

which may be verified by differentiation. As above, we assume that the initial magnetization is entirely z directed and has been normalized to 1. We refer to Eq. [12] as the small tip-angle approximation for M_z.

The final tag pattern $M_z(\mathbf{x})$ is found by evaluating Eq. [12] for $t = T$, which, in the k-space path notation, results in the final pattern

$$M_z(\mathbf{x}) \approx 1 - \tfrac{1}{2}\left| \gamma \int_{\mathbf{K}} p(\mathbf{k}) e^{i\mathbf{x}\cdot\mathbf{k}} d\mathbf{k} \right|^2. \quad [13]$$

A Fourier transform identity then yields

$$M_z(\mathbf{x}) \approx 1 - \tfrac{1}{2}\gamma^2 \int_{\mathbf{K}} R_p(\mathbf{k}) e^{i\mathbf{x}\cdot\mathbf{k}} d\mathbf{k}, \quad [14]$$

where $R_p(\mathbf{k})$ is the autocorrelation function of $p(\mathbf{k})$ given by

$$R_p(\mathbf{k}) = \int_{\mathbf{K}} p(\mathbf{u}) \bar{p}(\mathbf{u} - \mathbf{k}) d\mathbf{u}. \quad [15]$$

We refer to Eq. [14] as the *tagging k-space approximation.* It shows that the critical information needed to approximate a tag pattern is not the k-space path of the pulse sequence, but the autocorrelation function of that path.

This observation may be used in two ways: in the forward direction to analyze pulse sequences, and in the inverse direction to design pulse sequences. We summarize these two uses in algorithmic form as follows.

Algorithm 1: The forward problem. Given a pulse sequence, the approximate tag pattern may be found using the following steps:

1. Compute $p(\mathbf{k})$, the k-space path of the pulse sequence.
2. Compute $R_p(\mathbf{k})$, that path's autocorrelation function.
3. Compute the inverse Fourier transform of $R_p(\mathbf{k})$ in Eq. [14] to find the pattern $M_z(\mathbf{x})$.

Algorithm 2: The inverse problem. Given a desired tag pattern, a corresponding pulse sequence may be found using the following steps:

1. Compute the Fourier transform of $1 - M_z(\mathbf{x})$ to determine $R_p(\mathbf{k})$.
2. Find a path $p(\mathbf{k})$ that has the autocorrelation function $R_p(\mathbf{k})$ (spectral decomposition).
3. Determine the pulse sequence corresponding to that path.

4. RESULTS

4.1. SPAMM Analysis

The benefits of the tagging k-space approximation become readily apparent when the forward algorithm is applied to the SPAMM pulse sequence. We begin with the SPAMM path (Eq. [10]) and calculate its autocorrelation function $R_p(k)$, as illustrated in Fig. 2 for the 1-1 SPAMM sequence. The general solution is given by

$$R_p(k) = \frac{1}{\gamma^2} \sum_{l=1-N}^{N-1} \sum_{m=1}^{N-|l|} \theta_m \theta_{m+|l|} \delta(k - l\Phi). \quad [16]$$

Then, using $R_p(k)$ in the tagging k-space Eq. [14] yields the approximate SPAMM pattern

$$M_z(x) \approx \sum_{m=0}^{N-1} \hat{\alpha}_m \cos(m\Phi x), \quad [17]$$

where

$$\hat{\alpha}_m = -\sum_{l=1}^{N-m} \theta_l \theta_{l+m} \quad m = 1, \ldots, N-1$$

$$\hat{\alpha}_0 = 1 - \tfrac{1}{2} \sum_{l=1}^{N} \theta_l^2. \quad [18]$$

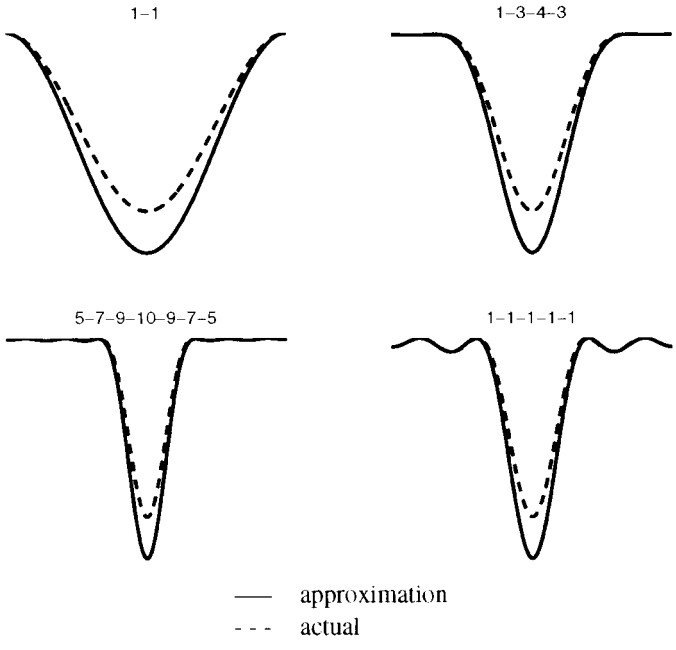

FIG. 3. Comparison of approximated tag profiles using Eq. [17] and actual tag profiles from Bloch equation simulation for four SPAMM sequences. The number and relative amplitudes of RF pulses are denoted above each plot. Actual amplitudes were adjusted to produce a total tip angle of $\pi/2$.

We immediately observe two benefits of this approximation. First, unlike excitation *k*-space, tagging *k*-space provides a direct expression for $M_z(x)$ that correctly predicts a symmetric sequence of $2N - 1$ impulses in *k*-space and a tag pattern identical in form to the exact solution; compare the cosine series of Eq. [17] to Eq. [3]. Second, unlike the exact solution, tagging *k*-space provides a simple expression, Eq. [18], for the coefficients in the cosine series. These advantages make our approximation of the SPAMM pattern quite useful for simulations and for optimizing pulse sequences.

In Fig. 3, we demonstrate the accuracy of the approximation for several SPAMM patterns. The figure superimposes the exact tag profiles and those obtained using the tagging *k*-space approximation. In an image, each of these profiles would repeat with a spatial frequency of Φ, producing the parallel stripes. Overall, the approximation is excellent at predicting overall shape, although it slightly overestimates tag depth.

4.2. Selective Presaturation

Analysis of the SPAMM pulse sequence shows that the tagging *k*-space approximation works well for pulse sequences that encode discrete *k*-space with an array of impulses. The tagging *k*-space approach is also useful for analyzing continuous *k*-space paths produced by continuous RF pulse sequences. Furthermore, tagging *k*-space is not limited to the analysis of tagging sequences, but may be applied to general selective presaturation sequences, where the goal is suppression of unwanted signal regions.

To demonstrate, we analyze the pulse sequence in Fig. 4a, which may be used to selectively presaturate broad regions around a central slab of interest. The continuous RF waveform used is an appropriately scaled version of the function

$$\left(\operatorname{sinc}^2 t - \frac{4}{9}\operatorname{sinc}^2\frac{2}{3}t\right)\sin 2\pi t$$

truncated after the third sidelobe and windowed with a Hamming window. The resulting saturation profile is depicted in Fig. 4b.

We first analyze the sequence with the excitation *k*-space approximation, computing the centered *k*-space path depicted in Fig. 4c. Using this path in the excitation *k*-space approximation (Eq. [9]) we obtain the approximate excitation pattern depicted in Fig. 4d, which is not indicative of the true presaturation pattern. We then analyze the sequence using our approximation (Eq. [14]), computing first the autocorrelation of the *k*-space path, as shown in Fig. 4e. Using this function in the tagging *k*-space approximation, we obtain the approximate

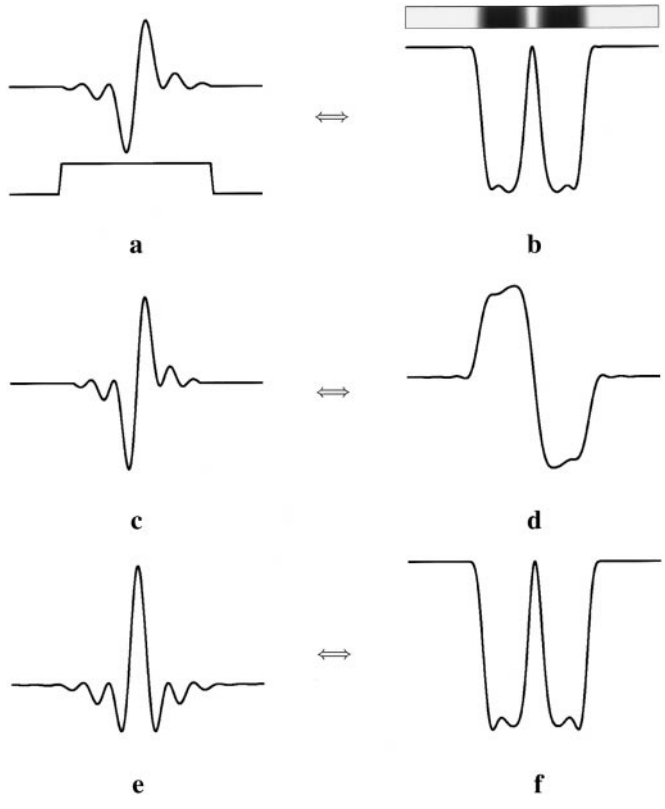

FIG. 4. A *k*-space analysis of selective presaturation showing (a) the RF and gradient pulse sequence, (b) the resulting double presaturation band around a narrow slab of interest, shown as an image and a profile, (c) the *k*-space path of this sequence, (d) the excitation *k*-space approximation of the *y*-directed pattern, (e) the autocorrelation of the path, and (f) the tagging *k*-space approximation of the *z*-directed saturation pattern, which closely matches the true pattern (b).

pattern depicted in Fig. 4f, which is nearly an exact match to the true pattern. From this, we conclude that the tagging *k*-space approximation is useful in the analysis of pulse sequences with continuous waveform excitation and for general selective presaturation.

4.3. VTAG Sequence Design

Turning to the design of pulse sequences, we now consider a recently developed tag pattern called variable separation tagging (VTAG), in which the spacing between tag lines is allowed to vary (*5*). The ability to tailor the local tag spacing to the expected local motion leads to better sampling of that motion—particularly when analyzing the myocardium of the left ventricle. To illustrate, Fig. 5a depicts the previously proposed pulse sequence for generating a pattern with separations of 5, 4, 3, 3, 3, 3, 3, and 3 pixels (*5*).

One problem with VTAG as proposed, however, is that long, time-consuming sequences of pulses are required in order to produce the desired patterns. For example, the sequence of Fig. 5a consists of 50 RF pulses lasting nearly 30 ms. For practical use, VTAG patterns generated with fewer RF pulses are desirable. One obvious means of reducing the number of RF pulses is simply to remove all but the largest pulses from the proposed sequence. Removing enough pulses to produce significant time savings, however, leads to a pattern with highly inconsistent tag depths. By applying our *k*-space analysis method, on the other hand, we can reduce the time required to apply this pattern, while maintaining consistent tag depths.

To demonstrate, the original VTAG sequence was developed by defining a desired 1D excitation pattern $M_{xy}(x)$ that produces tag lines at the desired spacing. Then, the Fourier coefficients of $M_{xy}(x)$ were calculated to determine the corresponding path through *k*-space depicted in Fig. 5b, which led directly to the pulse sequence. As we have shown, however, $M_z(x)$ is actually determined by the autocorrelation of the path, depicted in Fig. 5c.

Using spectral decomposition techniques (see the Appendix), we designed an alternative pulse sequence—using only 15 RF pulses instead of 50—that produces nearly the same autocorrelation. The sequence is depicted in Fig. 6 along with its *k*-space path and autocorrelation $R_p(\mathbf{k})$. The precise tip angles of the RF pulses and the relative areas of the gradient pulses are provided in Table 1. A comparison of the resulting brightness profiles for the original sequence and our sequence (Fig. 7) shows they are nearly indistinguishable. The benefit of the new sequence is that it constructs essentially the same pattern in well under half the time. We also attempted to use the spectral decomposition algorithm described in the Appendix to further shorten the sequence, but found that the tag pattern rapidly degraded when fewer than 15 pulses were used.

4.4. Multidimensional Tag Patterns

The tagging *k*-space approximation may also be used to describe the encoding of multidimensional *k*-space, thereby predicting multidimensional tag patterns. We envision the development of 2D SPAMM sequences where the orientations of the gradient pulses are permitted to vary in the *xy* plane. For example, a six-pulse 2D SPAMM sequence with three gradient orientations is depicted in Fig. 8, along with its 2D *k*-space path and autocorrelation function. Applying our *k*-space analysis to this sequence, we first recognize that $R_p(k_x, k_y)$ is a

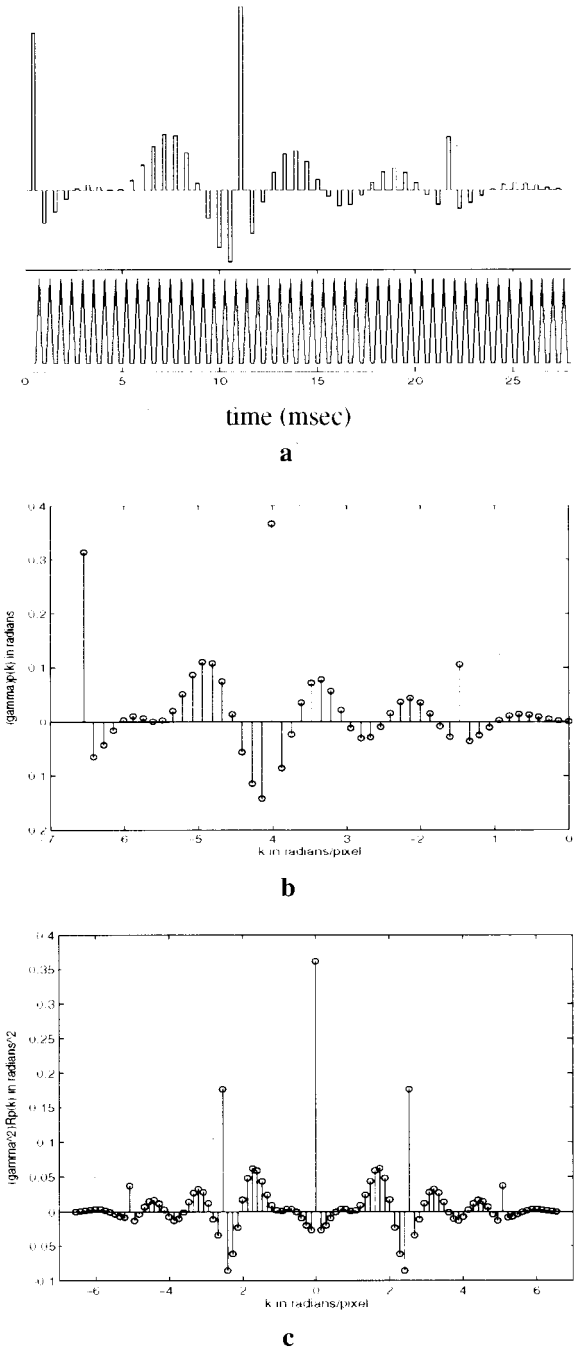

FIG. 5. A *k*-space analysis of the 5, 4, 3, 3, 3, 3, 3, 3 VTAG pattern showing (a) the RF and gradient pulse sequences proposed in (*5*), (b) the corresponding *k*-space path, and (c) the autocorrelation function of the path.

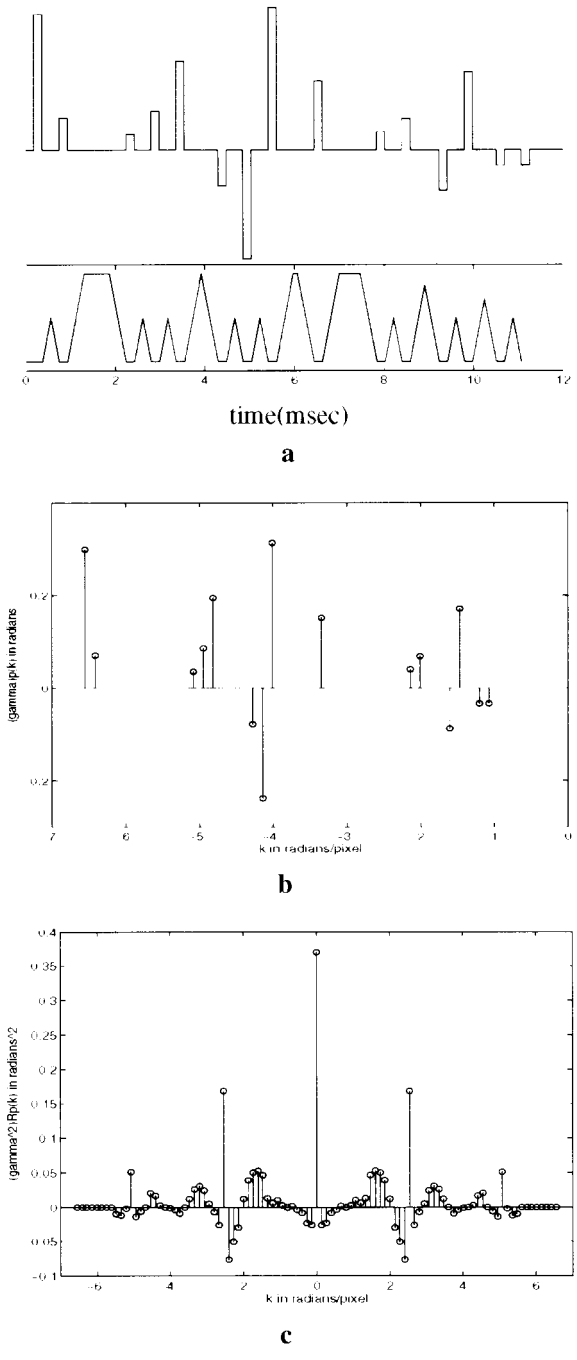

FIG. 6. A shorter pulse sequence for 5, 4, 3, 3, 3, 3, 3, 3 VTAG generation showing (a) the new pulse sequence, (b) the corresponding *k*-space path bearing little resemblance to Fig. 5b, and (c) the autocorrelation function of the path, which is nearly identical to Fig. 5c.

windowed version of $S_\Phi(k_x, k_y)$, the hexagonal 2D sampling function depicted in Fig. 8d, where the windowing function is approximately given by the Gaussian function

$$W(k_x, k_y) = 15\left(\frac{\pi}{18\gamma}\right)^2 e^{-(2/3\Phi^2)(k_x^2+k_y^2)}. \qquad [19]$$

The inverse Fourier transform (IFT) of $R_p(k_x, k_y) \approx S_\Phi(k_x, k_y)W(k_x, k_y)$ is a convolution of the IFT of $S_{\Phi(k_x}, k_y)$ and the IFT of $W(k_x, k_y)$. Therefore, Eq. [14] gives

$$M_z(x, y) \approx 1 - 1.44S_{4\pi/\Phi\sqrt{3}}(y, x) * e^{-(3\Phi^2/8)(x^2+y^2)} \qquad [20]$$

and the resulting tag pattern is predicted to be a hexagonal array of dark spots separated by $4\pi/\Phi\sqrt{3}$. The brightness profile of the spots is predicted to be Gaussian with width parameter $(1/\Phi)\sqrt{8/3}$. The accuracy of this estimate is demonstrated in Fig. 9, which shows the true pattern and its brightness profile, with the predicted Gaussian shape superimposed for reference.

This new tag pattern has potential uses in motion tracking because it is functionally equivalent to tracking the intersections in a tagging grid, an approach taken in (*15*), among others. The array of spots, however, has some distinct advantages over the grid. First, the well-defined circular features in the new pattern would likely permit better localization by image processing routines. Second, the easily recognized spots would likely prove simpler for segmenting those within the myocardium. Finally, the hexagonal distribution of the spots is better for sampling the roughly circular geometry of the LV in short axis sections.

5. DISCUSSION

The *k*-space interpretation of tagging leads to several important implications regarding pulse sequences. We demonstrated that the *k*-space encoding of M_z is essentially determined by the autocorrelation of the *k*-space path function. Because many paths often exist with similar or identical autocorrelations, this leads to a great deal of flexibility in designing pulse sequences. This flexibility led to the simplification of the

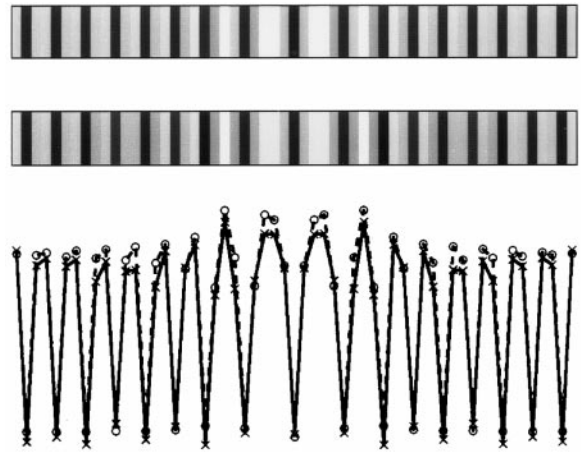

FIG. 7. Comparison of simulated pixel intensities and profiles for the pulse sequence of Fig. 5 (upper strip and ○) and for the sequence of Fig. 6 (lower strip and ×).

TABLE 1
Tip Angles in Radians and Relative Gradient Areas for the New Variable Separation Tag Pattern Proposed

Pulse	Tip	Gradient	Pulse	Tip	Gradient	Pulse	Tip	Gradient
1	0.3117	1	6	−0.0816	1	11	0.0716	3
2	0.0737	10	7	−0.2478	1	12	−0.0919	1
3	0.0372	1	8	0.3263	5	13	0.1784	2
4	0.0896	1	9	0.1582	9	14	−0.0354	1
5	0.2029	4	10	0.0419	1	15	−0.0347	—

VTAG sequence in particular and may simplify other complicated sequences as well. Our tagging *k*-space approximation also implies that a desired tag pattern $M_z(\mathbf{x})$ is only achievable if the Fourier transform of $1 - M_z(\mathbf{x})$ can be expressed—at least approximately—as the autocorrelation of a function $p(\mathbf{k})$. These two simple rules—applicable to pulse sequence design—were not clearly evident prior to this analysis.

A somewhat less obvious and perhaps more important realization made possible by this analysis quantifies what had been a qualitative observation regarding tagging. In general, sharply defined tag features are desirable for accurate localization. Beyond a certain degree of sharpness, however, diminishing returns have been observed. Tagging sequences, therefore, have been chosen to produce features that are fairly sharp, but not overly sharp. The phenomenon of diminishing returns is clearly explained by a *k*-space interpretation—very sharp features correspond to high spatial frequencies in *k*-space and those high frequencies are not imaged. Encoding such high frequency regions of *k*-space is an inefficient use of time, the resulting loss of high frequency energy reduces the contrast-to-noise ratio of the tags, and the frequency truncation can severely distort the tag pattern, counteracting any a priori optimization of the tag pattern. Therefore, tagging sequences should be designed to encode only those areas of *k*-space that will subsequently be imaged.

To limit *k*-space encoding to the region being imaged, our tagging *k*-space approximation provides a concrete rule regarding the *k*-space path of the pulse sequence. Autocorrelation effectively doubles the width of any function; therefore the *k*-space path of the tagging sequence should only be *half* as wide as the region of *k*-space to be imaged. For example, the distance from the first to the last pulse in the SPAMM path (Eq. [10]) is $(N - 1)\Phi$. If d is the width of a pixel, then the number of pulses N should be chosen so that $2(N - 1)\Phi \leq 2\pi/d$, which is the width of *k*-space to be imaged. This leads to the rule that

$$N \leq 1 + \tfrac{1}{2}g, \qquad [21]$$

where $g = 2\pi/\Phi d$ is the tag separation in pixels. In the typical range of four to six pixel tag separations, this implies that SPAMM sequences with more than three or four pulses will result in frequency truncation.

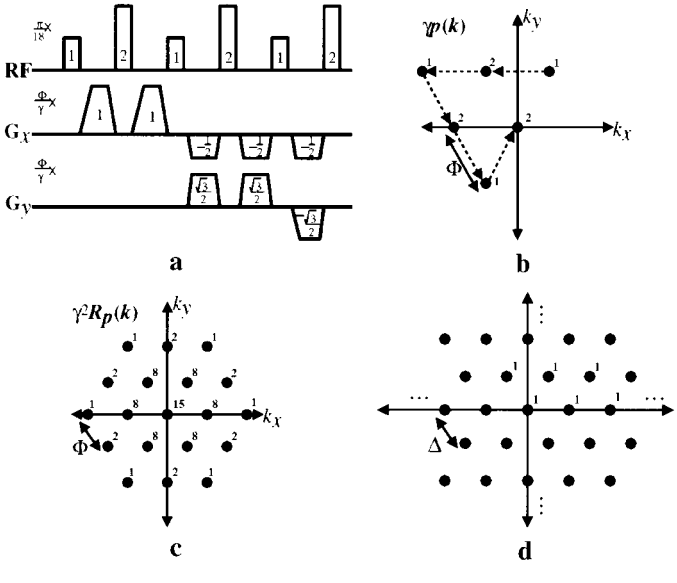

FIG. 8. A 2D *k*-space analysis showing (a) a 2D SPAMM sequence, (b) its *k*-space path, and (c) the autocorrelation of the path. The autocorrelation is a scaled and Gaussian windowed version of (d) the 2D sampling function $s_\Delta(\ldots)$, a hexagonal array of unit impulse functions with a separation of Δ. The dots represent impulse functions with the indicated heights times $\pi/18$ in (b) and $(\pi/18)^2$ in (c).

6. CONCLUSION

We demonstrated that our *k*-space interpretation of tagging is an effective tool for analyzing, designing, and optimizing pulse sequences for tagging and other selective presaturation applications. Our fundamental conclusion is that tag patterns are determined not by the *k*-space path of a pulse sequence, but by the autocorrelation function of that path. We showed that this autocorrelation function accurately approximates the tag pattern through a simple Fourier transform expression.

Using our approximation, we analyzed and designed pulse sequences for SPAMM, VTAG, and 2D SPAMM tags and for selective presaturation of regions around a central slab. These examples demonstrate that the approximation is effective for both the discrete *k*-space paths encountered in tagging and the continuous *k*-space paths more often encountered in selective presaturation applications. They also show that the method

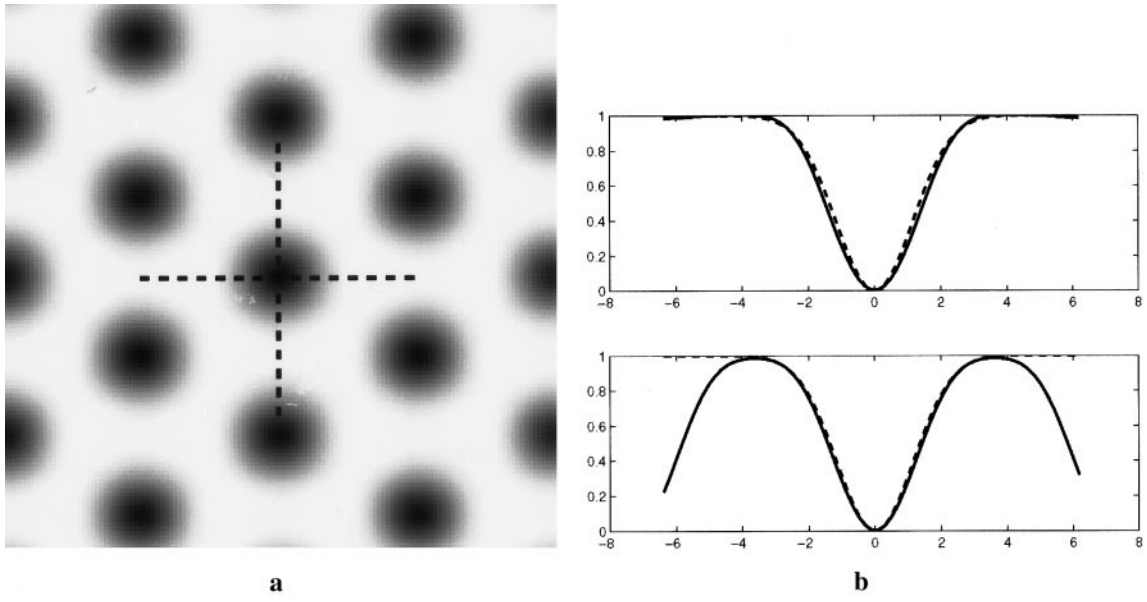

FIG. 9. Simulation of the 2D SPAMM sequence in Fig. 8 produces (a) a tag pattern consisting of black dots with (b) brightness profiles depicted along the two indicated axes. Also shown in (b) as a dotted line is a Gaussian profile of the same width given by the approximation. The x axis is distance with units of Φ.

applies in one or several dimensions. Finally, as demonstrated by the shortened VTAG sequence, the approximation aids in optimizing pulse sequences.

In addition to the improved VTAG sequence, we also presented a new 2D SPAMM sequence that produces a hexagonal array of spots. This new pattern may prove superior to tag grids for tracking 2D point motion in tagged images. Our approximation also provided new insights into the 1D SPAMM pattern. In particular, we showed that the k-space interpretation leads to a simple tag profile expression, Eq. [17], consisting of a sum of cosines, which may be used for rapid simulation of tag patterns. It also leads to a simple rule for choosing the number of RF pulses needed for a given tag separation, given by Eq. [21].

APPENDIX

Spectral Decomposition

In Section 5.1, the following problem arises: We have a discrete autocorrelation function $R_p^*[k]$ of length $2N - 1$ and we wish to determine a discrete pulse sequence $p_m[k]$—generally of length N—that reproduces this autocorrelation function to high accuracy. Our goal is therefore to find $p_m[k]$ that minimizes

$$f(p_m) = \sum_{k=1-N}^{N-1} |R_p^*[k] - R_p[k]|^2, \qquad [22]$$

where

$$R_p[k] = \sum_{l=|k|+1}^{N} p_m[l]\bar{p}_m[l - |k|],$$
$$k = 1 - N, \ldots, N - 1. \qquad [23]$$

While similar problems have been addressed for applications from wavelets and filter banks (see (*16*)) to stochastic modeling (see (*17*)), we add the unique constraint that only m of the n pulses may be nonzero. Thus, the problem involves not only optimizing the pulse amplitudes, but also the arrangement of the nonzero pulses.

To illustrate, consider the autocorrelation function depicted in Fig. 5c, for which $N = 50$. In Fig. 6b, we depict a sequence with 15 nonzero entries with an autocorrelation function that closely approximates Fig. 5c. Optimally locating these 15 pulses is not tractable analytically. Likewise, an exhaustive search is not computationally feasible because there are 2.25×10^{12} possible arrangements of 15 pulses in 50 slots.

To identify the 15-pulse sequence, we applied the following procedure to the problem. Our basic approach is to build the sequence one pulse at a time, alternately selecting the "best" location to add a pulse, and then reoptimizing the pulse amplitudes for this choice. The procedure terminates based on a user-defined stopping criterion, which may be a prespecified value for m, a measure of the quality of the fit, or a visual inspection of the simulated pattern. We do not claim the procedure is optimal, nor can we guarantee that it will con-

verge. It has, however, performed well in practice, in particular identifying the new VTAG sequence.

Mathematically, let S_m be the set of indices l over which a given sequence $p_m[l]$ is allowed to be nonzero, $l = 1, \ldots, N$, and let $P(S_m)$ be the set of all pulse sequences with nonzero entries only in positions S_m. We attempt to find S_m^* and $p_m^*[k]$, the optimal arrangement and pulse amplitudes, using the following algorithm.

Algorithm 3: Constrained spectral decomposition.

- Step 0. Initialize $m = 1$, $S_1 = \{1\}$, $p_1[1] = \sqrt{R_p^*[0]}$, and $p_1[k] = 0$ for $k = 2, \ldots, N$.
- Step 1. Find $l^* = \underset{l=1,\ldots,N, l \notin S_m}{\operatorname{argmax}} \left| \frac{\partial}{\partial p[l]} f(p) \right|_{p=p_m}$.
- Step 2. Set $S_{m+1} = \{S_m, l^*\}$.
- Step 3. Find $p_{m+1} = \underset{p \in P(S_m+1)}{\operatorname{argmin}} f(p)$ (see below).
- Step 4. Set $m = m + 1$. If stopping criterion not met, go to Step 1.

In this algorithm, the initialization in Step 0 is selected because the resulting $p_1[k]$ is the optimal one-pulse sequence. Then, Step 1 essentially finds the pulse location where an added pulse will result in the greatest improvement in the fit—that is, the pulse location that results in the largest derivative of the function to be minimized. In Step 3 the optimal pulse amplitudes $p_{m+1}[k]$ are found using gradient descent, with $p_m[k]$ as an initialization.

REFERENCES

1. E. A. Zerhouni, D. M. Parish, W. J. Rogers, A. Yang, and E. P. Shapiro, Human heart: Tagging with MR imaging—a method for noninvasive assessment of myocardial motion, *Radiology* **169,** 59–63 (1988).
2. L. Axel and L. Dougherty, MR imaging of motion with spatial modulation of magnetization, *Radiology* **171,** 841–845 (1989).
3. E. R. McVeigh, MRI of myocardial function: Motion tracking techniques, *Magn. Reson. Imaging* **14**(2), 137–150 (1996).
4. J. Pauly, D. Nishimura, and A. Macovski, A *k*-space analysis of small-tip-angle excitation, *J. Magn. Reson.* **81,** 43–56 (1989).
5. E. R. McVeigh and B. D. Bolster Jr., Improved sampling of myocardial motion with variable separation tagging, *Magn. Reson. Med.* **39,** 657–661 (1998).
6. A. A. Young, D. L. Kraitchman, L. Dougherty, and L. Axel, Tracking and finite element analysis of stripe deformation in magnetic resonance tagging, *IEEE Trans. Med. Imaging* **14**(3), 413–421 (1995).
7. L. Axel and L. Dougherty, Heart wall motion: Improved method of spatial modulation of magnetization for MR imaging, *Radiology* **172,** 349–350 (1989).
8. T. J. Moser and M. B. Smith, A DANTE tagging sequence for the evaluation of translational sample motion, *Magn. Reson. Med.* **15,** 334–339 (1990).
9. S. Chandra and Y. Yang, Simulations and demonstrations of localized tagging experiments, *J. Magn. Reson. B* **111,** 285–288 (1996).
10. I. Sersa and S. Macura, Excitation of arbitrary shapes by gradient optimized random walk in discrete *k*-space, *Magn. Reson. Med.* **37,** 920–931 (1997).
11. M. Shinnar and J. S. Leigh, Inversion of the Bloch equation, *J. Chem. Phys.* **98**(8), 6121–6128 (April 1993).
12. J. Pauly, P. Leroux, D. Nishimura, and A. Macovski, Parameter relations for the Shinnar–Leroux selective excitation pulse design algorithm, *IEEE Trans. Med. Imaging* **10**(1), 53–65 (1991).
13. W. R. Crum, E. Berry, J. P. Ridgway, U. M. Sivananthan, L. Tan, and M. A. Smith, Frequency-domain simulation of MR tagging, *J. Magn. Reson. Imaging* **8,** 1040–1050 (1998).
14. W. S. Hinshaw and A. H. Lent, An introduction to NMR imaging: From the Bloch equation to the imaging equation, *Proc. IEEE* **71,** 338–350 (1983).
15. A. A. Young and L. Axel, Three-dimensional motion and deformation of the heart wall: Estimation with spatial modulation of magnetization—a model-based approach, *Radiology* **185,** 241–247 (1992).
16. G. Strang and T. Nguyen, "Wavelets and Filter Banks," Wellesley–Cambridge Press, Wellesley, MA (1997).
17. M. H. Hayes, "Statistical Digital Signal Processing and Modeling," Wiley, New York (1996).